NASA's Newest Orbital Debris Ground-based Telescope Asset: UKIRT

S. M. Lederer[1*], J.M. Frith[2], H. M. Cowardin[2], B. Buckalew[2]

[1]NASA Orbital Debris Program Office, NASA/JSC, Houston, TX 77058, USA
[2]JETS Jacobs Technology

ABSTRACT

In 2014, NASA's Orbital Debris Program Office (ODPO) gained access to the United Kingdom Infrared Telescope (UKIRT). This will extend our spectral coverage into the near- (0.8-5μm) and mid- to far-infrared (8-25μm) regime. UKIRT is a 3.8m telescope located on Mauna Kea on the Big Island of Hawaii. At nearly 14,000-feet and above the atmospheric inversion layer, this is one of the premier astronomical sites in the world and is an ideal setting for an infrared telescope. An unprecedented one-third of this telescope's time has been allocated to collect orbital debris data for NASA's ODPO over a 2-year period.

UKIRT has several instruments available to obtain low-resolution spectroscopy in both the near-IR and the mid/far-IR. Infrared spectroscopy is ideal for constraining the material types, albedos and sizes of debris targets, and potentially gaining insight into reddening effects caused by space weathering. In addition, UKIRT will be used to acquire broadband photometric imaging at Geosynchronous Earth Orbit (GEO) with the Wide Field Camera (WFCAM) for studying known objects of interest as well as collecting data in survey-mode to discover new targets. Results from the first stage of the debris campaign will be presented.

The combination of this ground-based telescope with NASA's optical assets will yield spectral coverage ranging from 0.3 – 25 μm, allowing orbital debris to be studied in depth across a wider wavelength range in the visible and IR than ever previously studied by ODPO. By expanding the methods for surveying, detecting, and characterizing orbital debris, we can better model the debris environment and ultimately gain insight into how to mitigate potential collisions for future missions.

1. INTRODUCTION

In 2014, NASA's Orbital Debris Program Office (ODPO) gained access to a 3.8-meter infrared telescope located in one of the best astronomical sites in the world. In 2012, The Space Technology Facility Council (STFC) of the United Kingdom announced that it was seeking new ownership and management of their United Kingdom Infrared Telescope, UKIRT, located on the Big Island of Hawaii on Mauna Kea (19.8º N, 155.5W) [Fig. 1]. At nearly 14,000 ft., this observatory boasts clear skies, and is often located above the atmospheric inversion layer. This site offers exceptionally dry atmospheric condition that typically yields humidity levels less than 20% and often 5-10% or lower. This is especially important when observing at infrared (IR) wavelengths as the atmospheric water vapor acts to absorb light in the targeted wavelength regime. In the IR, the very stable atmosphere at this site combined with the facility and telescope design can result in astronomical 'seeing' (resolution) as low as 0.2-0.4″. NASA's ODPO has been granted a subset of guaranteed time using this telescope for the purposes of characterizing orbital debris.

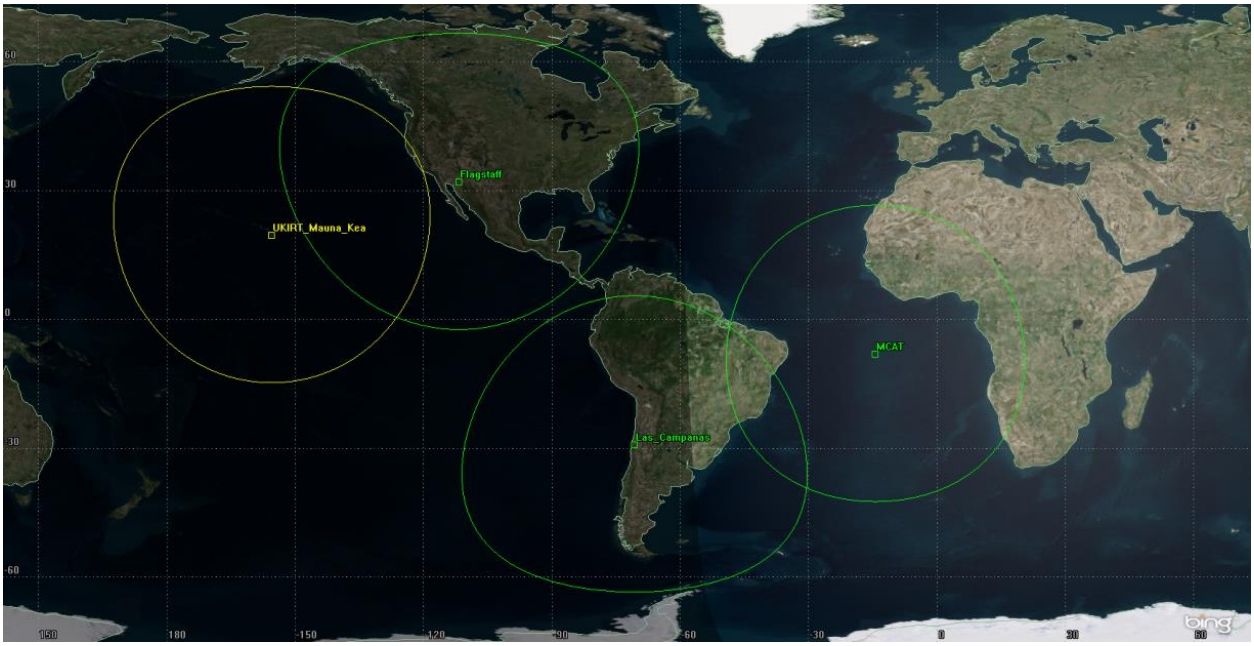

Fig. 1. Viewing Geometries of current NASA Assets, including UKIRT on Mauna Kea, and optical assets MCAT on Ascension Island, and MODEST at Cerro Tololo Interamerican Observatory (CTIO) in Chile. Data have also been collected for NASA's ODPO by the US Naval Observatory in Flagstaff, Arizona.

Estimates of the sizes of debris are critical to understanding and assessing the risk to functional spacecraft. While radar allows a direct measurement of debris sizes, objects at Geosynchronous Earth Orbit (GEO) require a significant amount of energy to be detected with radar. As a consequence, by using visible-band photometry, the brightness of an object in the visible is measured, an albedo (brightness) assumed, and sizes of objects inferred. This is only accurate if the material type is known, which is generally not the case for debris. Observations taken with the 8-25 μm thermal imager-spectrometer, Michelle, could be used to calculate the size of an object directly if the object is bright enough at mid-infrared (IR) wavelengths. Once true size is directly measured, it could then be used in conjunction with visible-band observations to calculate the true albedo in the visible and material type constrained.

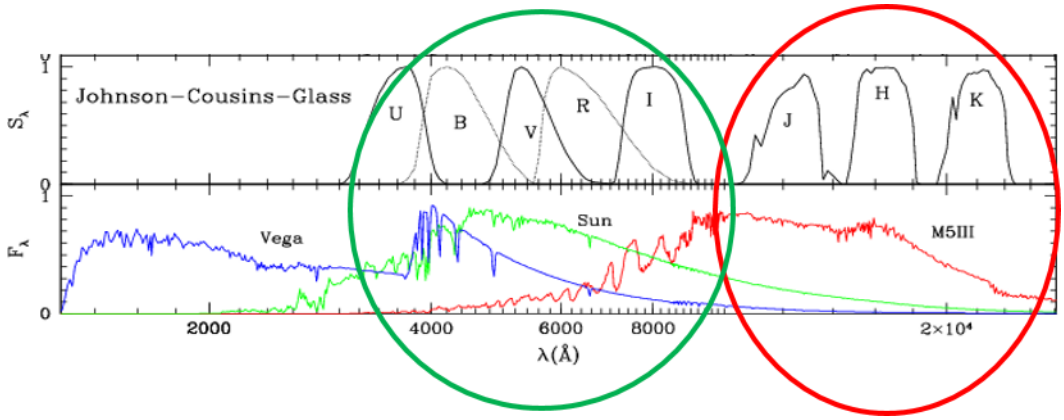

Fig. 2. Spectra of a blue (Vega), yellow (Sun) and red (M5III) star compared with visible-band Johnson -Cousins filters (circled in green) and infrared bands (circled in red) [1].

An estimate of the size of an object that can be detected in the infrared is dependent on a number of factors. The sun is significantly fainter in the infrared than in the visible (Fig. 2), giving the infrared a distinct disadvantage. Reflectance spectra taken with NASA's Infrared Telescope Facility (IRTF) demonstrates how flux might vary with wavelength for a variety of objects, including examples of a spacecraft, a rocket body (ISU R/B(2)a) and a piece of Titan Debris (Fig. 3).These objects' fluxes can be significantly greater in the infrared than in the visible. All else being equal, if an object were 4x brighter in the infrared than the visible, we could detect objects that are 2x smaller

using infrared techniques. The tendency for the object's reflectivity to be higher in the infrared combined with UKIRT's large mirror help account for the drop in solar flux.

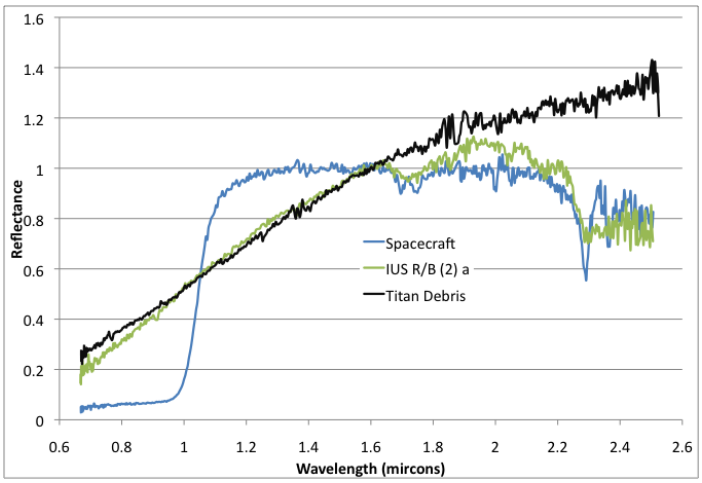

Fig. 3. Reflectance Spectra taken with the 3.0-meter IRTF telescope in Hawai'i comparing a spacecraft, a rocket body, and debris, scaled at 1.6 µm. In September 2014, the UKIRT 1-5µm Imager SpecTrometer (UIST) will be used to collect similar data in the 1-2.5 µm regime.

In addition, a database of IR spectra (1-2.5µm bandpass) of potential debris materials can be compared with telescopic data to constrain the composition of observed objects. For example, absorption features attributed to C-H bonds are seen near 1.7 and 2.2-2.3µm in Fig. 3 and are attributed to solar cell materials [2]. Combining the 1 – 2.5 µm spectral finger printing to assess material type with the optical (visible-band) data should strengthen the identification of debris materials.

Space reddening may be predominant in the IR but it is not well understood [3, 4]. UKIRT will allow us to investigate what is causing this phenomenon. Brightness, and therefore accurate size distribution calculations, is affected by reddening so understanding this should improve our size estimation techniques.

As the telescope is not designed to track at LEO (Low Earth Orbit) rates, the observations described herein focus on objects located in GEO. UKIRT is well suited to study targets in GEO and has undergone a transformation allowing the telescope to track objects in this orbital regime. This telescope gives NASA the opportunity to extend investigations of debris from the traditional radar and visible bands used to detect and study debris into the infrared. This presents a golden opportunity to more directly measure and infer tumble rates, sizes, and compositional information allowing one to constrain materials comprising the targets. With better insights into material type and size estimates, NASA's ODPO can better quantify the risk to active spacecraft.

2. INSTRUMENTATION

UKIRT is equipped with a suite of instruments allowing for both imaging as well as high and low resolution spectroscopy to be obtained (Fig. 4, Table 1). The instruments include: (1) the Cooled Grating Spectrometer 4 (CGS4), a 0.8 – 5 µm 2D grating spectrometer, allowing for high resolution spectroscopy; (2) Michelle, a mid-infrared imager/spectrometer operating from 8 – 25 µm, which can also be used for polarimetry; (3) the UKIRT Fast-Track Imager (UFTI), a 1 – 2.5 µm camera; and (4) the UKIRT 1 – 5µm Imager SpecTrometer (UIST), which also has a polarimetry option. While UFTI is more sensitive than UIST, it has a smaller field-of-view and is not a spectrometer. UIST is the instrument of choice for near-IR low-resolution spectra in the 1 – 2.5 µm regime; (5) the Wide Field Camera (WFCAM) boasts a large field of view for an infrared array instrument, and was designed specifically to allow for a large-scale survey. This is useful for discovering uncorrelated targets (UCTs).

Fig. 4. The UKIRT facility (*left*) is home to a 3.8m infrared telescope (*right*), shown here with WFCAM mounted on the telescope at prime-focus (the large black cylindrical instrument). Photos courtesy Tom Kerr (facility) and Paul Hirst,(telescope), Joint Astronomy Centre (JAC).

Table 1: UKIRT instrumentation details.

Instrument	Spectral Range (μm)	Spectral Resolution	FOV	Polarimetric Option?
CGS4 (echelle spectroscopy)	0.8–5	37,000		N
Michelle (imaging)	8–25		67″ × 50″	Y
Michelle (spectroscopy)	8–25	200 to 30,000		Y
UFTI	1–2.5		90″	Y
UIST (imaging)	0.8–5		1′ or 2′	Y
UIST (slit spectroscopy)	0.8–5	500 to 6,000		Y
UIST (integral field spectroscopy)	0.8–5	500 to 6,000	3.5″ × 6.5″	Y
WFCAM	1–2.5		4 × (13″ × 13″)	N

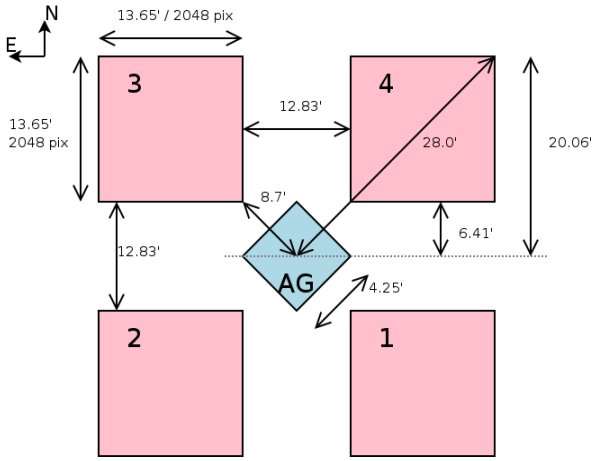

Fig. 5. WFCAM focal plane. All observations were targeted to fall on array 3, the cleanest array.

WFCAM was designed for surveying the sky with an interesting footprint on the sky (Fig. 5). Four 2048 x 2048 pixel HAWAII-2 detector chips are designed to collect data at infrared wavelengths. Each chip spans 13.65′ x 13.65′. The 18 μm pixels yield 0.4″/pixel resolution on the sky. Each chip is oriented as a square with large gaps, 12.83′ from the edge of one chip to edge of the adjacent chip. Embedded in the center of the 4 chip layout, but located within the gaps, is a fifth chip oriented as a diamond. This small fifth array allows auto-guiding (AG) on an object using visible wavelengths with a beam-splitter in the path of the telescope sending the visible light to the AG. The AG chip is 4.25′ x 4.25′. A complete image 0.75° x 0.75° results by shifting the array four times on-sky. (For further details, see Kendrick et al., this meeting). A set of broadband filters (ZYJHK) covers 0.83 – 2.37μm [5].

3. DATA and ANALYSIS

WFCAM has been the sole instrument on UKIRT for the past six years, and was used to collect data of debris and spacecraft targets for ODPO during the first semester of 2014. JHK filters were used for all observations. Additional observations will be made with this instrument in the coming semesters. Data were taken +/- 5 days around new moon in April, May, and June, 2014. A subset of observations are described herein, including (1) three IDCSPs (Initial Defense Communications Satellite Program; 86 cm in diameter), SSN 2220, 2652, and 3289 (Fig. 6); (2) the Meteosat Second Generation (MSG) cooler cover (0.8 m^2), SSN 29106, and (3) the MSG baffle cover ($2m^2$), SSN 29676.

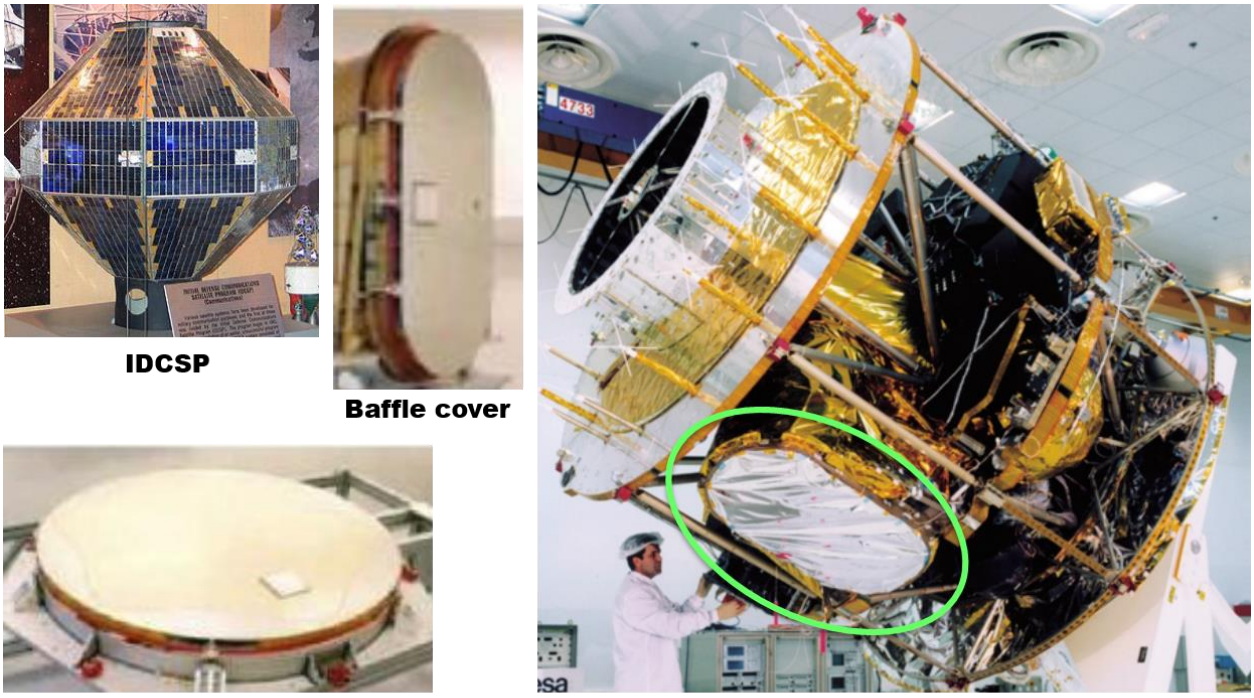

Fig. 6. Targets for WFCAM included (clockwise) an IDCSP [6], the MSG cooler cover and the MSG baffle cover.

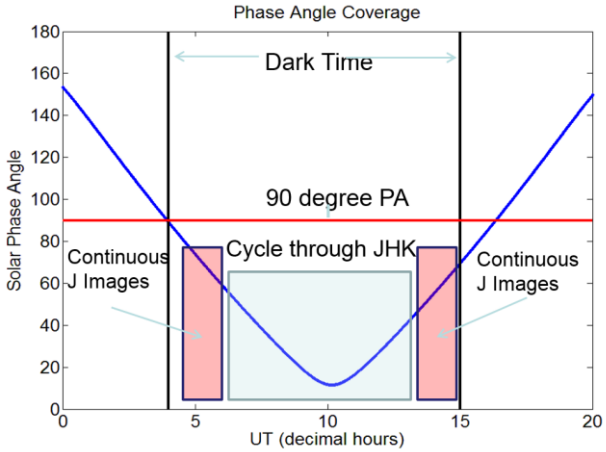

Fig. 7. Data for a given object were taken while the solar phase angle (PA) was less than 90 degrees with a cadence of continuous J-band filter images, followed by J-H-K sequences cycled, followed by continuous J-band images.

The cadence to take the data was designed in the following manner: For the debris and satellite data, the telescope tracked at the non-sidereal rate expected for the target. Continuous J-band images were taken for 30 minutes at the beginning and the end of each sequence to allow an analysis of the rotational period/tumbling of a subset of objects. Sequences of JHK-JHK-JHK were cycled between the J-band images when J-band continuous data were taken, ensuring cycling occurred before/after the object reached its minimum solar phase angle (SPA). Else continuous cycling of JHK images were taken throughout the night. Most objects were detected easily with 10-second integration times in all filters. Some of the fainter debris targets, such as the cooler cover, required 15-second integrations.

Because WFCAM has such large gaps between arrays, one must take a sequence of images and patch them together to create a spatially complete image. In the case of satellites that are point sources, this is not strictly necessary. The targets were centered on array 3 (the cleanest array) and those data are the focus of these analyses. Because it is possible that other debris might be found in the field surrounding our targets, the data were taken in such a way that the observations could be patched together for future analyses to search for uncorrelated targets not found in the SSN catalog. Further analyses are required to search for UCTs.

A sequence of images tracking at sidereal rates is also taken regularly to obtain data of star fields for the purpose of photometrically calibrating the data. The sidereally tracked data were taken at the start and end of each set of JHK images.

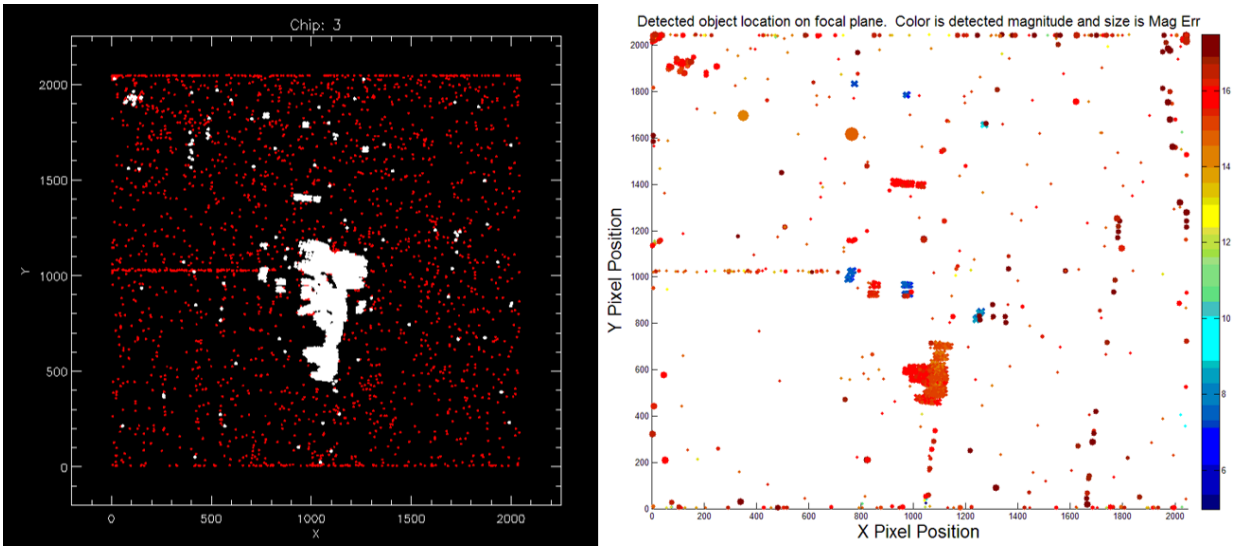

Fig. 8. Chip 3 before and after 'cleaning' demonstrating the need for additional criteria to be placed on determining 'real' detections of debris. This highlights some of the challenges in infrared data processing.

The data were reduced and processed by the Cambridge Astronomical Survey Unit pipeline. This was modified to detect streaked objects in the images to (1) detect the targets that were moving when the telescope tracked sidereally (i.e. with the motion of the stars) for the earliest data (before tracking GEO non-sidereally was possible), and (2) to remove streaked objects in the sky (stars) when the telescope tracked at the object's non-sidereal rate. (Details on the data reduction procedure can be found at [7, 8] and references therein).

Data reduction of the WFCAM data is an involved process. Over 95% of the initial 'detections' indicated by the pipeline process are false detections caused by defects in the arrays, cosmic ray hits, and other artifacts caused by particularly bright objects producing artificial detections (Fig. 8). The pipeline processing procedures vastly reduced the number of false detections greatly eliminating hundreds of thousands of false detections, but many remained and had to be filtered out after the data were processed. This elimination of artifacts was done by using a combination of analyzing the ellipticity of the detection, the FWHM, and chip location constraints. Resulting magnitude uncertainties are approximately ± 0.1 magnitudes in each filter for all data.

Though the data have been processed, the individual images are not yet easily accessible. Only the text output of a subset of the full dataset from the pipeline has been analyzed, which became available only weeks ago. As such, analysis is ongoing and results herein are preliminary.

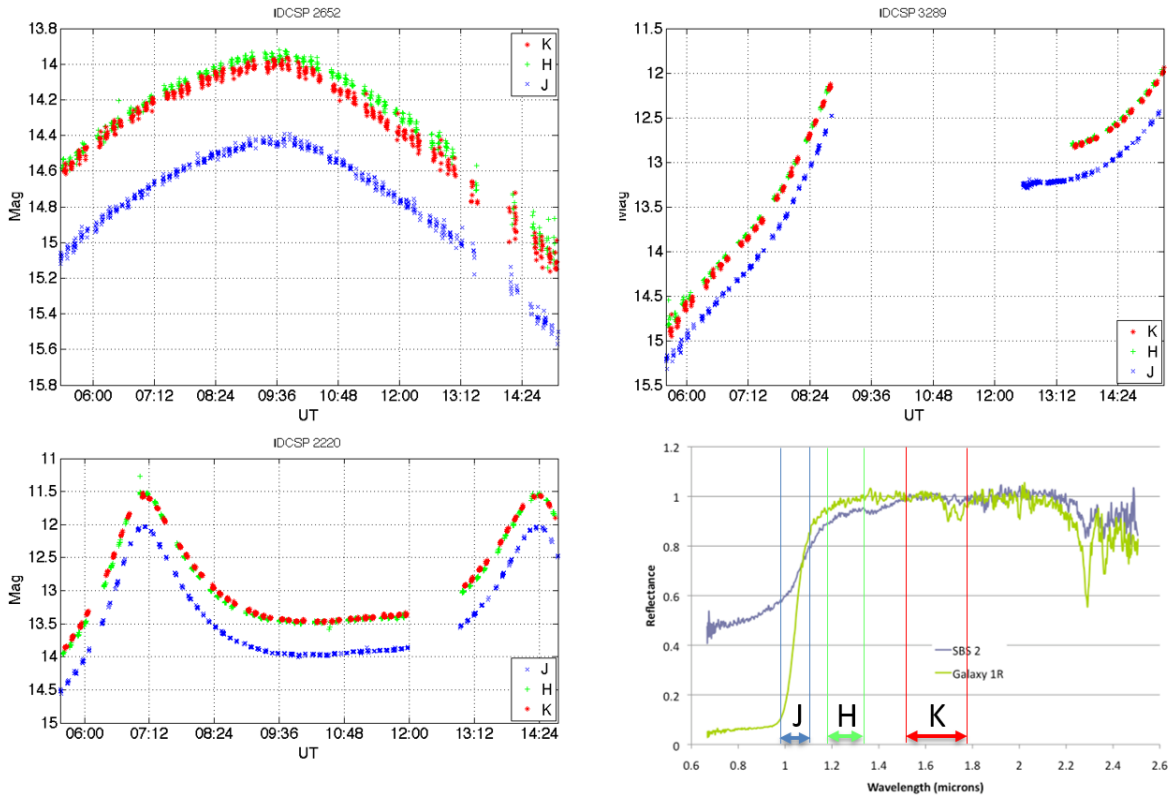

Fig. 9. Plots of the JHK magnitude versus UT for three separate IDCSPs (SSN 2652, 3289, and 2220). A comparison spectrum of two satellites covered in solar panels (SBS 2) and with large solar arrays deployed (Galaxy 1R) with the bandpasses of the JHK filters over-plotted [2]. Spectra were taken with the IRTF telescope in Hawai'i.

IDCSPs are 26-sided spin-stabilized polygon spacecraft, 86 cm in diameter, covered with solar panels (Fig. 6) and launched into slightly sub-synchronous orbits with periods of 22.2 ± 0.2 h [6, 9]. One might expect the data taken by WFCAM to mimic what is expected for a spacecraft with a significant solar panel component. Many IDCSPs were observed including SSN 2652, 3289, and 2220. Two spectra of spacecraft covered in solar panels (SBS 2) and with large solar arrays deployed (Galaxy 1R) are shown for comparison with the bandpasses of J (0.97 – 1.07 μm), H (1.17 – 1.33 μm), and K (1.49 – 1.78 μm) over-plotted [2]. Given the similarity of SBS 2's exterior, one would expect the J magnitudes to be similarly fainter than HK for all IDCSPs. Plots of magnitude versus UT shown in Fig. 9 for three IDCSPs confirm clearly that in all cases, the J magnitude is fainter than the H and K.

For such geometrically symmetric objects, the lightcurves are oddly different in both shape and amplitude. Further studies and modeling are required to determine why these originally spin-stabilized objects present such different lightcurves. It intimates that the objects may no longer be spin-stabilized, and or that they are presenting different viewing geometries of the satellite (e.g. pole-on versus equator-on versus a tumbling state). The excellent temporal resolution of the data aids in this exercise, suggesting that the objects are not tumbling, but rather are presenting different orientations of each spacecraft. Modeling will aid in constraining the possible tumble/orientation arguments.

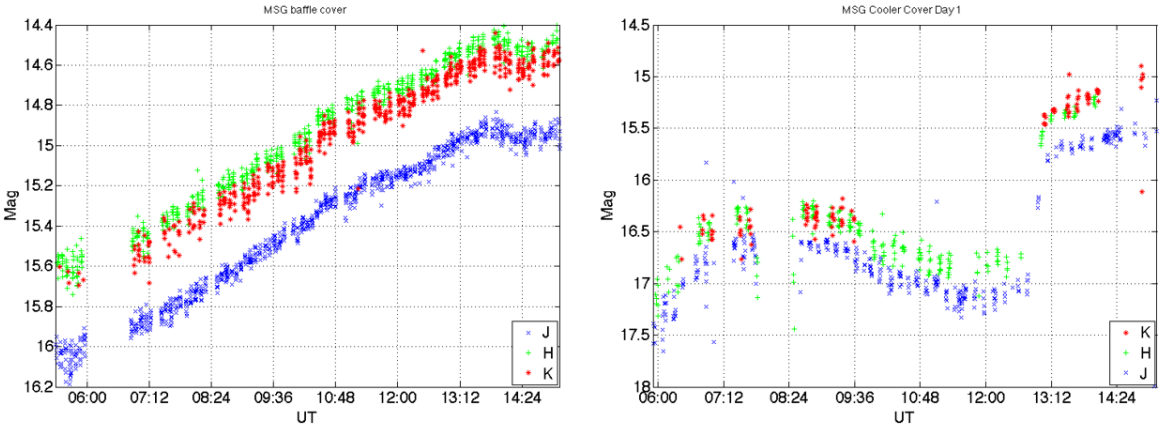

Fig. 10 Plots of the JHK magnitude versus UT for the MSG baffle cover (left) and cooler cover (right).

Data were also taken of the Meteosat Second Generation (MSG) baffle cover (SSN 29676) and cooler cover (SSN 29106) that were both ejected from the spacecraft after launch (Fig. 6). Not surprisingly, the cooler cover, which is the smallest of the targets presented, is also the faintest. Rotation/tumbling cannot be easily extracted from the data, but the variation in magnitude with the rotation/tumble is may be indicated by the vertical spread, ~0.3mag, in each set of data points (Fig. 10). For comparison, the 3σ uncertainty in magnitude is ± 0.1 mag, less than the observed spread in magnitude. A clear change in the brightness trend with UT is observed in all data.

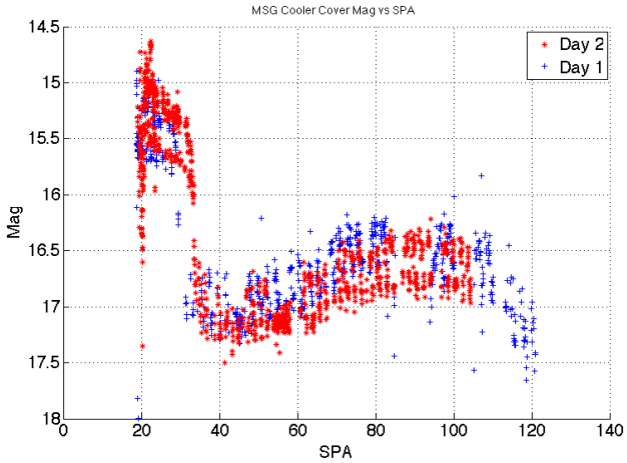

Fig. 11. Brightness (magnitude) versus solar phase angle (SPA) for one of the MSG cooler covers on two separate days (May 27 and May 31, 2014).

In the case of the cooler cover, a flat round disk, the SPA is decreasing as UT increases (Fig. 11). All else being equal, one would expect that the brightness of an object would increase as the SPA decreases as is generally indicated by the data, though there is a peak at 90 degrees SPA. The cause of the sharp drop in magnitude at 20 degrees SPA is not obvious. One might expect that the precipitous drop in magnitude at 20 degrees SPA could be explained by the object going into shadow. However, the data were taken near the solstice when the Earth's shadow does not interfere with low inclination objects, including this one. Further studies modelling the behaviour of the cooler cover will need to be conducted to better understand the data.

4. SUMMARY

NASA's newest telescope asset, UKIRT, an IR telescope located on Mauna Kea, offers new insights into studying debris. Wavelength coverage from the current optical assets is now extended into the infrared and affords NASA's ODPO access to data ranging from 0.4 µm to 25 µm. A work in progress, the data presented here comprise a subset of the first 20 nights of data collected over 2 months (April-May 2014). Five objects were observed with the

WFCAM instrument on UKIRT, offering a glimpse into the properties of debris. JKH data of three IDCSPs are consistent with the IRTF spectra of spacecraft either surrounded by, or presenting large fractions of solar panels. All IDCSP J-band photometry is consistently fainter than the HK counterparts, as expected for an object covered in solar panels. The inconsistency in lightcurve shape hints at either tumble-states, or different viewing geometries of the objects. The very small vertical spread, however, suggests the objects are each presenting different viewing geometries. On the other hand, the reverse is true for the cooler and baffle covers. The vertical spread in magnitude is greater than the errors and hints at very rapid tumble rates.

These data demonstrate the high frequency data acquisition capabilities and potential contribution to understanding debris. Data have also been collected on various debris targets with both WFCAM and UIST and will be the focus of future presentations and papers. The data pipeline, once finished, will allow additional insights, including correlations with SPA and rotational period analyses. Ultimately, the infrared regime will offer direct access to constraining tumble rates, sizes, and compositional information, leading to a better understanding of material type and risk to functional spacecraft.

5. ACKNOWLEDGEMENTS

Special thanks to Matt Bold and Rick Kendrick of Lockheed Martin; Tom Kerr, Watson Varriccatt, Sam Benigni, Eric Moore, Tim Caroll, and the UKIRT staff at the Joint Astronomy Centre; Dr. Richard Green and the University of Arizona, for their collaborative efforts toward modifying UKIRT to boldly venture inward in space to track small man-made objects orbiting the Earth. Special thanks also to Drs. Mike Irwin, Greg, Madsen, University of Cambridge, and the Institute for Astronomy staff at the University of Edinburgh, Royal Observatory for their hard work in streamlining the pipeline for extracting data on moving-objects-in-the-sky.

6. REFERENCES

1. Girardi L., Bertelli, G., Bressan, A., Choisi, C., Groenewegen, M.A.T., Marigo, P., Salasnich, B., Weiss, and A., Theoretical isochrones in several photometric systems. I. Johnson-Cousins-Glass, HST/WFPC2, HST/NICMOS, Washington, and ESO Imaging Survey filter sets, *Astron. Astrophys.*, Vol 391, 195-212, 2002**.**
2. Abercromby, K.J., Abell, P. and Barker E., Reflectance Spectra Comparison of Orbital Debris, Intact Spacecraft, and Intact Rocket Bodies in the GEO Regime, *5th European Conference on Space Debris, March 30 – April 2, ESOC, Darmstadt, Germany*, 2009.
3. Abercromby, K., Guyote, M., Okada, J., Barker, E., Applying Space Weathering Models to Common Spacecraft Materials to Predict Spectral Signatures, *2005 AMOS Technical Conference*, Wilea, Maui, Hawaii. 5-9 September, 2005.
4. Jorgensen Abercromby, K., Guyote, M., Okada, J. Hamada, K., and Barker, E., Comparison of Ground Truth and Remote Spectral Measurements of the FORMOSAT and ANDE Spacecrafts, *2006 AMOS Technical Conference*, Wailea, Maui, Hawaii, 10-14 September, 2006.
5. Tokunaga et al., The Mauna Kea Observatories Near-Infrared Filter Set. II. Specifications for a New JHKL'M' Filter Set for Infrared Astronomy, *PASP*, Vol.114, 180-186, 2002.
6. http://www.placesaroundflorida.com/Cape_Canaveral_Florida/CCAFS/image17.cfm
7. http://www.ast.cam.ac.uk/~mike/casu/
8. Kendrick et al., GEO Belt Survey with WFCAM, *2014 AMOS Technical Conference*, Wilea, Maui, Hawaii. 10-12 September, 2014.
9. Lambert J.V. et al., A Search for the Lost IDCSP Constellation. *19th Space Control Conference*, 2001.